Pramana – J. Phys. (2020) 94:27
https://doi.org/10.1007/s12043-019-1895-z

Effects of the positions of scintillation detectors with fast scintillators and photomultiplier tubes on TOF–PET performance

ELIF EBRU ERMIS* and CUNEYT CELIKTAS

Physics Department, Faculty of Science, Ege University, 35100 Bornova, Izmir, Turkey
*Corresponding author. E-mail: elermis@hotmail.com

MS received 4 September 2019; accepted 23 October 2019

Abstract. The objective of this study is to improve the time resolution value of a coincidence spectrometer used in a time-of-flight–positron emission tomography (TOF–PET) system. This spectrometer is used in medical imaging systems. The coincidence spectrometer is manufactured by using a BC420-type plastic scintillator and R1828-01-type photomultiplier tube, and the time resolution value of the manufactured spectrometer is determined. The accuracy of the experimental results is determined using the FLUKA Monte Carlo simulation program. Detectors are first manufactured in this program. Experimental and simulation results are compared and are found to be in good agreement. Optimal positions of the detectors are investigated to improve the coincidence time resolution of the spectrometer. Time resolution improvement of the optimal detector positions enables higher time-of-flight (TOF) gain and spatial resolution, leading to better image quality, reduction in patient doses and detection of small lesions.

Keywords. Coincidence spectrometer; time resolution; time-of-flight gain; FLUKA Monte Carlo simulation program.

PACS No. 07.57.Kp

1. Introduction

Positron emission tomography (PET) is a medical imaging method that uses radioactive isotopes, to take the image of the part of a patient's body.

1.1 *Basic principles of PET*

PET is based on the coincidence detection of two 511 keV photons emitted in opposite directions following the annihilation of a positron and an electron. The physics of positron decay and annihilation is shown in figure 1 [1,2].

Several geometries have been applied in the design of the PET detector [3]. PET scanner generally consists of several rings of crystals. Each detector contains one or more large crystals followed by photomultiplier tubes (PMT). The crystal of the detector converts gamma photon energy into light photon energy [4]. PMT is a vacuum tube consisting of an input window, photocathode, focussing electrodes, electron multiplier and anode [5]. The function of PET is to generate images of the distribution of positron emitters *in vivo*, detecting the annihilation photons surrounding the patient by coincidence detectors. Scintillators, PMTs and timing resolution are significant factors in the PET performance.

1.2 *Benefits of TOF principles*

Some systems measure time-of-flight (TOF) under the assumption that annihilation can be localised along the line of flight of coincident photons by measuring the time of arrival of each photon at their opposing crystals for optimum resolution. The time difference is proportional to the difference in distances travelled by the two photons. TOF measurement is used to calculate the position of the event along the line connecting the detectors [4].

1.3 *Structure of the detector of the system*

The type and composition of scintillation crystals are of considerable importance in the detection. To improve the detection performance of PET detectors, many types

Published online: 10 January 2020

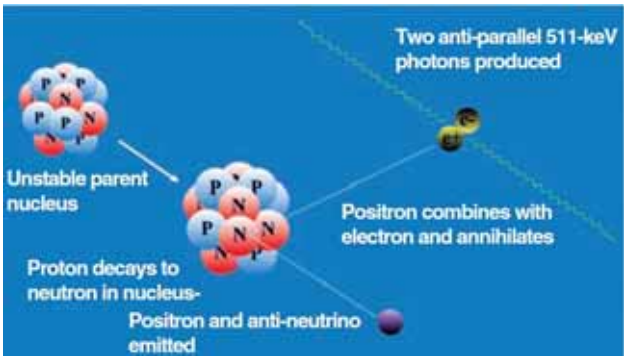

Figure 1. Physics of positron decay and annihilation [1].

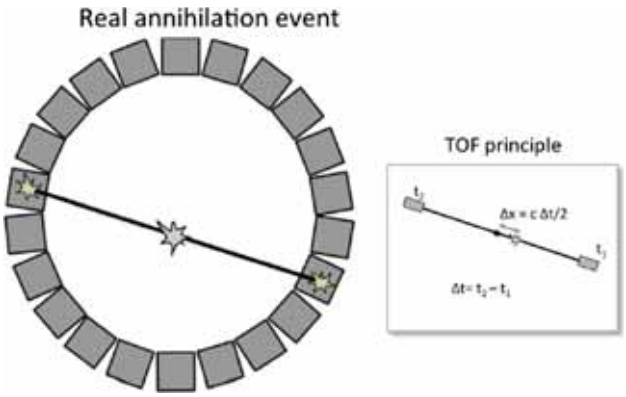

Figure 2. TOF–PET principles [14].

of scintillator materials have been suggested and implemented. Crystals that can provide high photon detection efficiency, short decay time and better energy resolution are highly preferred to improve timing characteristics of the PET detectors [3].

1.4 *Parameters used in the study of TOF-PET systems*

The time resolution of a detection system (Δt) can be determined by measuring the distribution of time delays between fast nuclear interactions. It is characterised by the full-width at half-maximum (FWHM) of a time spectrum [6]. FWHM is the width of the position of half of the maximum value of a peak distribution.

Time resolution values are used to define the spatial resolution (i.e., localisation uncertainty) of a TOF–PET system. The spatial resolution of the system (Δx) can be calculated as

$$\Delta x = c\Delta t/2, \tag{1}$$

where c is the speed of light and Δt is the time resolution of the system (figure 2) [7–13].

Spatial resolution is a characteristic quantity that describes the ability of an imaging system to reveal objects accurately in the two spatial dimensions of an image. The better is the spatial resolution, the better is the separation of two objects that are close to each other [15,16]. As the spatial resolution is a crucial parameter for a PET system, it is inevitable to improve it as much as possible. Functional images acquired with poor spatial resolution have several drawbacks, such as the likelihood of missing small metabolically active lesions, inaccurate quantitative measurements, and finally misdiagnosis [3].

Another important parameter for a TOF–PET system is the gain value (f). This value corresponds to the reduction in noise variance, where f is given by

$$f = D/\Delta x. \tag{2}$$

D is the size of the emission source or radial dimension of the object to be imaged [7–10,13,17].

1.5 *FLUKA Monte Carlo method*

The Monte Carlo (MC) calculations describe any technique in which complex models are evaluated by generating successive random samples and interpreting statistically the global results after numerous iterations [18].

One of the well-known set of MC codes is the FLUKA. It is based on FORTRAN language. Proton and electron accelerator shielding, target design, dosimetry and detector design can be simulated using particle transport and interactions with matter in this code [19,20].

1.6 *Objective of this study*

One of the most important parameters of a medical imaging system is the time resolution as this parameter considerably affects the image quality (i.e., spatial resolution) of the system. In this study, improved time resolution values were achieved by using a coincidence spectrometer consisting of a new generation scintillator and PMT that are more sophisticated than those presented in the previous studies [21,22].

2. Experimental

2.1 *Materials*

A ^{22}Na positron source is commonly used in PET imaging [23]. Therefore, a solid point ^{22}Na source with $\sim$5 μCi activity was used in this work.

Plastic scintillators are characterised by a relatively large light output and a short decay time. This makes the material suitable for fast measurements. In addition, plastic scintillators are the most popular scintillation

materials for use in TOF detectors. In this study, BC420-type (Saint-Gobain) scintillation crystal [24] was chosen which has a short decay time because this parameter is crucial in coincidence timing detection in PET imaging [3].

2.2 *Methods*

The primary focus of time spectroscopy is determining the relationship between the arrival times of particles emitted as a result of some event. Any detector having sufficient time resolution and response time can be used to build a time spectrometer. In most cases, a combination of the scintillator and PMT is used [25]. The constant fraction timing method was one of the timing measurement methods used in this study. Considerable information about the timing measurement method is provided in previous studies [26–28].

The experimental circuits used to achieve the time spectrum of ^{22}Na is shown in figure 3. We utilised two cylindrical (2-inch diameter and 2-inch height) plastic scintillators with a decay time of 1.5 ns. They were mounted on Hamamatsu R1828-01-type photomultiplier tubes. This type of PMT is suitable for PET applications [5,29]. The detectors were fed by an ORTEC-556-type power supply. The outputs of the detectors were connected to fast timing preamplifiers (FPAs, ORTEC VT120A). In fast timing applications, FPA is a device that generates high-performance and very fast linear signals from PMT [30]. The preamplifier outputs were sent to timing filter amplifiers (TFAs, ORTEC 454). The TFA provides an amplified signal and reduced high-frequency noise through a selectable integration time [31]. The outputs of TFAs were forwarded to constant fraction discriminators (CFD, ORTEC 463). One of the negative outputs of CFDs was connected to the 'start' input of the time-to-amplitude converter (TAC, ORTEC 566). The other negative CFD output was connected to the 'stop' input of the TAC through the delay unit (DL, ORTEC 425A). The DL was used to provide time for the delay between the 'start' and 'stop' inputs of the TAC. The TAC produces a pulse with an

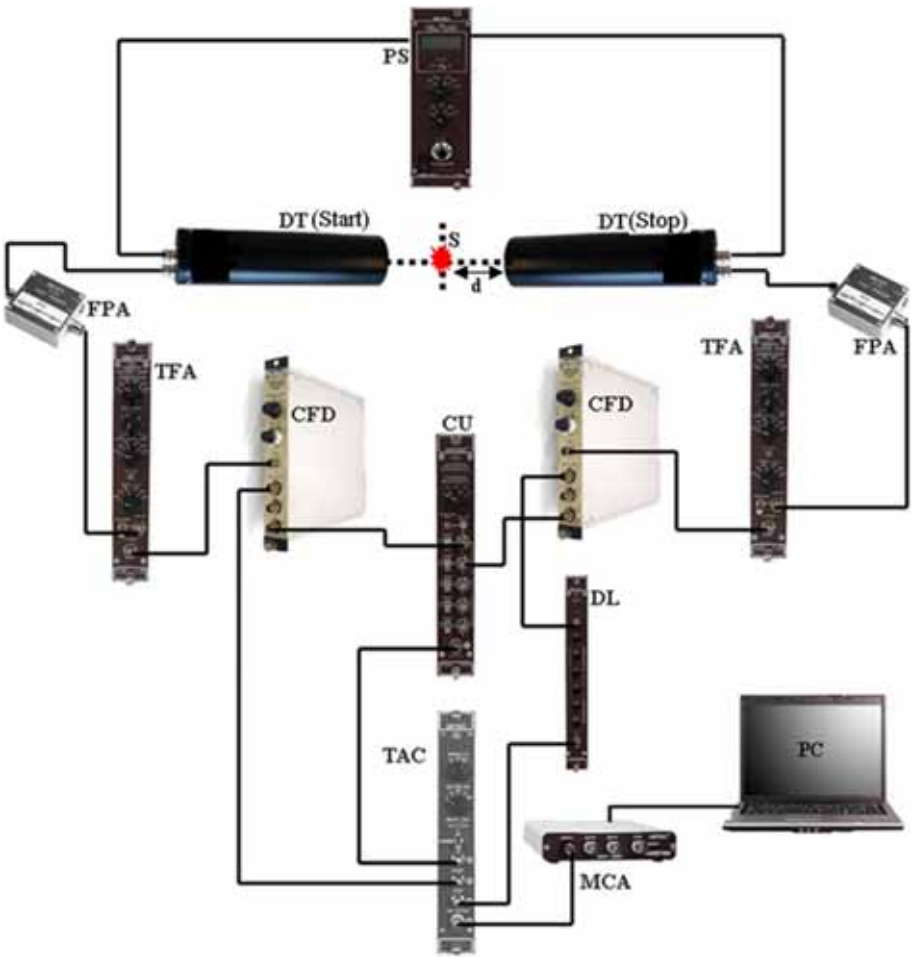

Figure 3. Experimental circuit of the spectrometer.

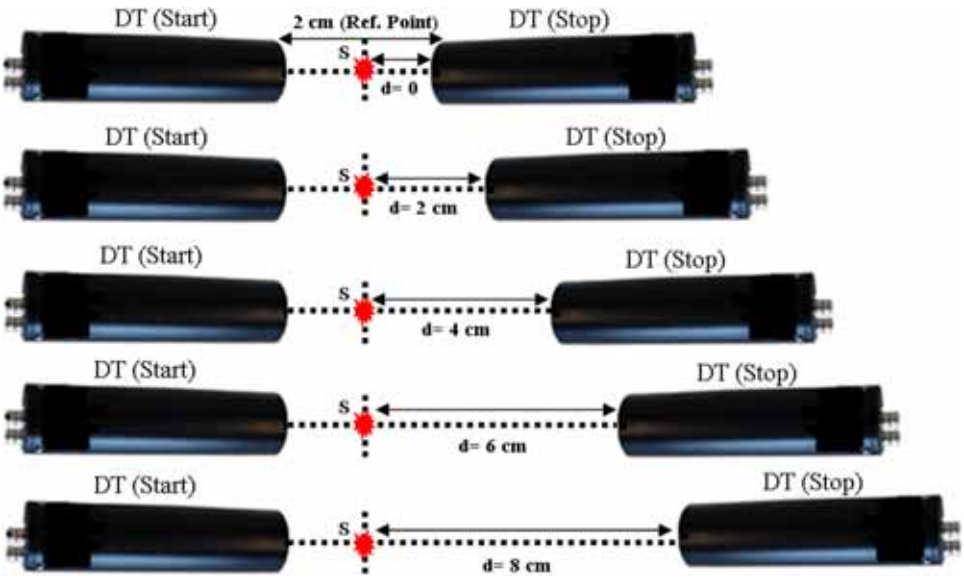

Figure 4. Positions of the detectors in the experiment.

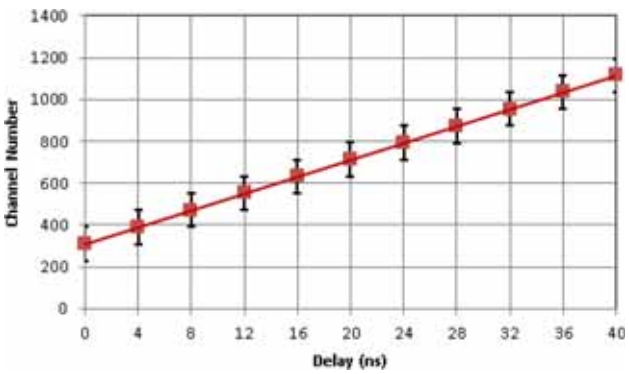

Figure 5. Time calibration of the detector (fitted time calibration = 49.692 ± 0.432 ps/ch).

amplitude proportional to the difference in the arrival times of the pulses [25]. The CFD positive outputs were forwarded to the coincidence unit (ORTEC 418A) to trigger the TAC's strobe input. Each event recorded by the two detectors gives rise to one TAC pulse. The distribution of the amplitudes of these pulses is called the timing spectrum [25]. A multichannel analyser (MCA, ORTEC Easy-MCA 2K) was used to achieve a coincidence time spectrum.

In the circuit shown in figure 3, the distance between the start and stop detectors was first set to a 2 cm position. The first position of the stop detector was chosen as a reference point ($d = 0$). Radioactive source, placed at the centre of the start and stop detectors in this reference position, was kept immobile during the measurements (figure 4).

In the first step of the experimental study, the time calibration of the MCA was performed in the reference position ($d = 0$). During the measurement, the TAC range was set to 100 ns, and the MCA conversion gain was selected as 2048 channels. The delay time was increased gradually from 0 to 40 ns in increments of 4 ns through the delay unit, which is shown in figure 6. In figure 5, the obtained time calibration graph is given. The time value per channel was calculated by taking the inverse of the slope of the calibration graph. This value was determined as 49.692±0.432 ps/ch. The TAC range and MCA conversion gain were also used in the time calibration to check the validity of the result from the calibration graph. A value of 48.828 ps/ch was obtained by dividing the TAC range (100 ns) by the MCA conversion gain (2048 channels). The slope of the graph and these calculation results were very similar.

The time difference between the start and the stop inputs of a TAC is known as the delay time. In this work, the optimum delay time was determined as 4 ns. As a result of the time calibration process, the best time resolution value was achieved at this delay time (figure 6).

In the second part of the study, the start detector was fixed, and the stop detector was moved away from its first position to the distances ($d = 2, 4, 6$ and 8 cm). The channel numbers corresponding to the timing peak positions were recorded vs. the position of the stop detector. The obtained results are provided in §4. The acquisition time was chosen as 300 s. The experiments were conducted in a dark room at a constant temperature of 23°C because ambient light and high temperature cause detector noise [26].

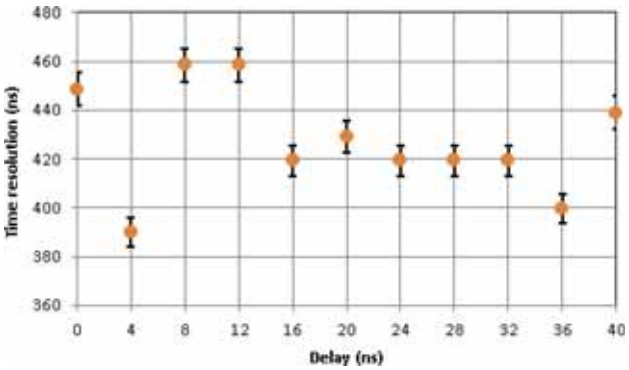

Figure 6. Optimal delay times.

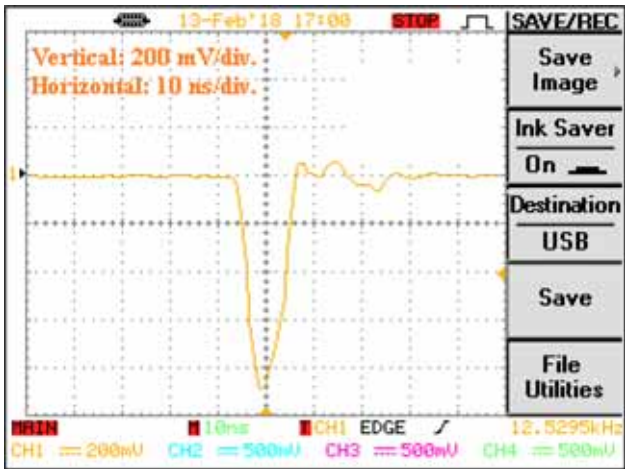

Figure 7. Output signal shape of the CFD.

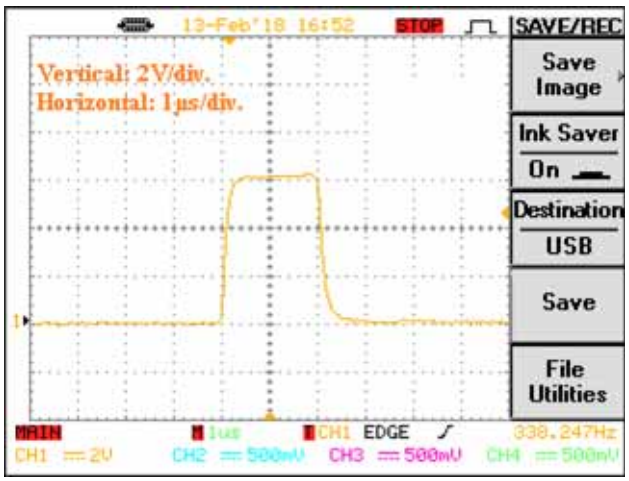

Figure 8. Output signal shape of the TAC.

CFD and TAC output signal shapes are shown in figures 7 and 8 respectively. These signal shapes were obtained from a digital oscilloscope (GW Instek GDS-2204).

3. Simulation

In this type of spectrometer, the FLUKA MC program was used to simulate detector construction to test its use. Physics lists and several scoring cards were used in the simulation process. Further information can be found in [19,20].

In the experiment, plastic scintillation detectors were used and their positions were simulated. The plastic scintillator and its plastic cover (2 mm) were kept in front of the scintillation crystal. Simulated detectors and their positions are shown in figure 9. A beam of 10^3 gamma photons of 511 keV was sent to both detectors. The distance between the detectors was altered in the experiment and coincidence counts were determined. In this calculation processes, the PRECISIO physics list was used because it serves as a better objective of this study than the other physics lists in the program. Finally, experimental and theoretical coincidence count results were compared.

In this program, maximum counts were determined for each detector distance. A comparison of the experimental and theoretical counts is provided in the following section.

4. Results

4.1 *Time resolution*

Figure 10 shows variations in peak positions with the distances from the reference point of the stop detector.

The obtained time resolution values vs. the distance from the reference point of the stop detector are shown in figure 11. Based on this comparison, the optimal position of the stop detector for the best coincidence time resolution value was determined (6 cm). In addition, the obtained time resolution values for each distance from the reference point of the stop detector are listed in table 1. Time resolution values in this table are the average of 5 iterations of each measurement.

4.2 *Spatial resolution and gain*

Spatial resolution values for the spectrometer (Δx) were calculated based on eq. (2). This calculation was repeated for each distance from the reference point of the stop detector to determine the best spatial resolution position. The obtained spatial resolution values are listed in table 2.

The gain value (f) of the spectrometer was also calculated according to eq. (2) at different distances from the reference point of the stop detector for two body types (heavy and average) and one body part

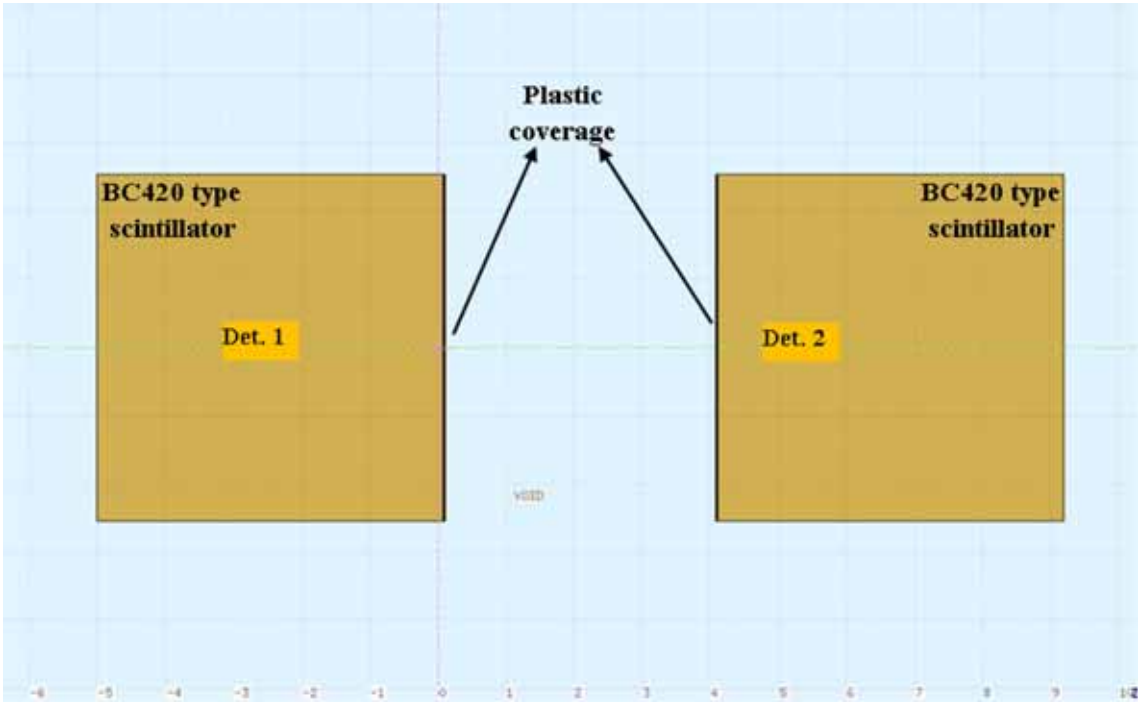

Figure 9. Simulated detector position in FLUKA MC program.

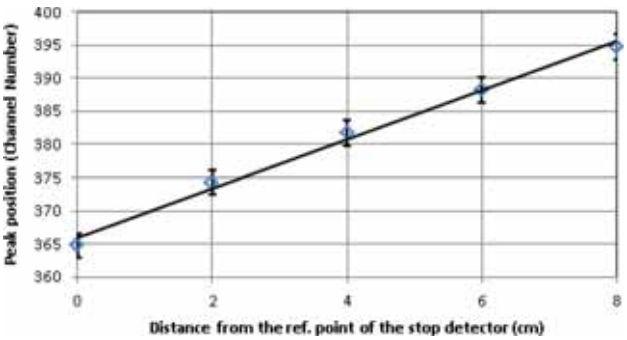

Figure 10. Peak position vs. distance from the reference point of the stop detector.

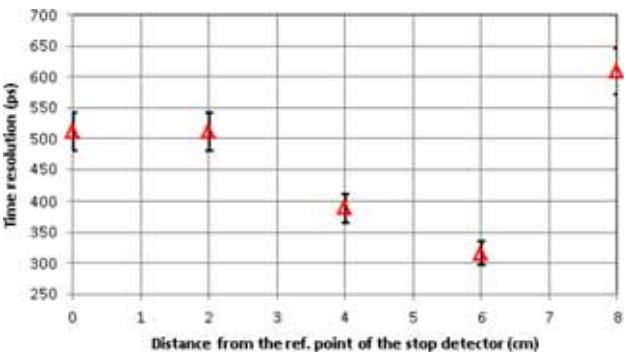

Figure 11. Time resolution values vs. distance from the reference point of the stop detector.

Table 1. Time resolution values for each distance from the reference point of the stop detector.

Distance from the reference point of the stop detector (cm)	Time resolution values (ps)
0.0	512 ± 0.044
2.0	512 ± 0.044
4.0	390 ± 0.051
6.0	317 ± 0.056
8.0	610 ± 0.041

Table 2. Spatial resolution values (Δx) of the coincidence system for each distance from the reference point of the stop detector.

Distance from the reference point of the stop detector (cm)	Spatial resolution values (Δx) (cm)
0.0	7.7
2.0	7.7
4.0	5.9
6.0	4.8
8.0	9.2

(brain). The radial dimension of the body type or imaged part is described by D. Values of D are 35, 27 and 20 cm for heavy, average bodies and the brain, respectively [10,14]. Calculated gain values for different values of D values at each distance are listed in table 3.

Table 3. Calculated gain value (f) and FWHM (timing resolution) for different values of D at each distance from the reference point of the stop detector.

Distance from the reference point of the stop detector [d, (cm)]	Gain value (f): heavy body	Gain value (f): average body	Gain value (f): brain	FWHM (timing resolution in ps)
0.0	4.56	3.52	2.60	512
2.0	4.56	3.52	2.60	512
4.0	5.98	4.62	3.42	390
6.0	7.36	5.68	4.21	317
8.0	3.83	2.95	2.19	610

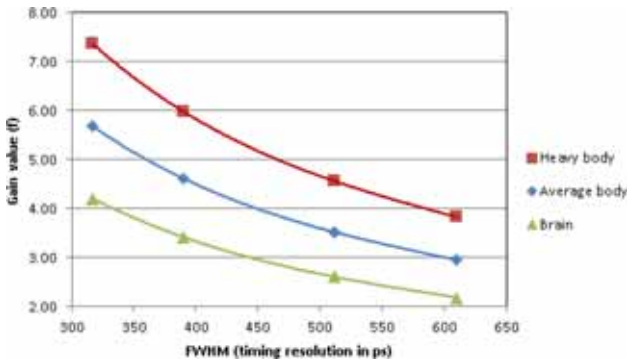

Figure 12. Variations in gain values (f) based on timing resolution values.

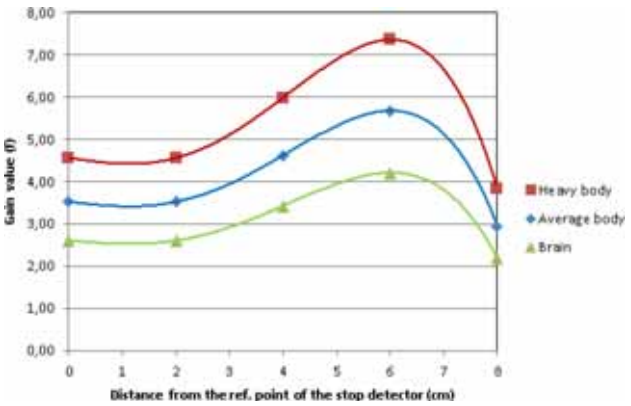

Figure 13. Variations in gain values (f) based on distance from the reference point of the stop detector.

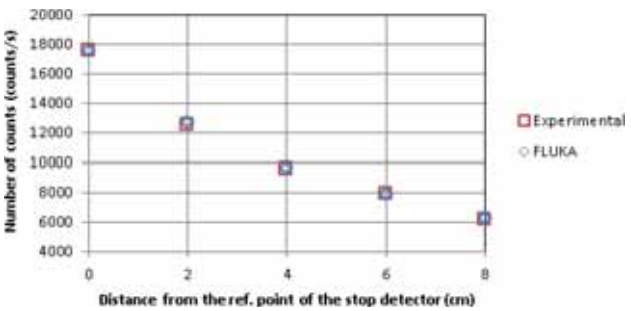

Figure 14. Comparison of the experimental and theoretical counts with respect to the distance from the reference point of the stop detector.

The variations in f based on timing resolution values of the spectrometer and distance from the reference point of the stop detector are shown in figures 12 and 13.

Because f depends on the time resolution as defined in eq. (2), values of f are plotted in figure 12 to determine the variation vs. time resolution.

In addition, values of f at different distances from the reference point of the stop detector were investigated to reveal the effect of distance between the patient and the detector based on the position of the stop detector in the TOF–PET system.

4.3 *FLUKA MC results*

The obtained theoretical coincidence counts through the FLUKA MC program as a function of different distances from the reference point of the stop detector (d) were determined. A comparison between the theoretical and experimental counts are shown in figure 14.

5. Discussion

As discussed in [3,32], TOF–PET measurement is directly affected by the time resolution of the coincidence system. For this reason, improvement of timing resolution was conducted in this study. The TOF measurement is used in current PET imaging. The main components of the system are scintillator, PMT and electronics. These components also have considerable importance for TOF–PET systems. Improvement of the time resolution value of these systems is achieved by using fast scintillators, fast PMTs and appropriate electronics [14].

Enhancement of time resolution values of the coincidence spectrometer has many advantages. First, the imaging time is reduced as a result of improving the time resolution value, which enables healthy tissue

and lesions to be clearly distinguished. The scintillation crystals that have faster decay times are used to enhance the time resolution values of the system [3,33]. Another important parameter of the TOF–PET system is to choose the most appropriate PMT for the scintillation crystal [33]. Therefore, a coincidence spectrometer consisting of very fast scintillators and PMTs is used, and excellent time resolution values are achieved in the constructed spectrometer. The present study reveals that the selection of the scintillation crystal and PMT as well as the position of the stop detector in the spectrometer, are critical to the performance of a TOF–PET system.

Timing in nuclear and particle physics corresponds to the measurement of very small time intervals. An example of its use is the TOF measurement. Constant fraction timing discrimination is the most efficient and versatile method available today [26]. Therefore, the constant fraction discrimination method is used to prevent the effects of degradation of time resolution values due to electronic noise in TOF–PET system electronics [12]. This method was used in our experiment based on this information.

Based on extensive literature research, three D values (i.e., radial dimensions of the object to be imaged) were chosen. In the references, D values for heavy body, average body and brain were given as 35, 27 and 20 cm, respectively [10,14].

Figure 12 shows that better timing resolution was obtained with higher f values. In other words, as the time resolution was enhanced, the gain and spatial resolution values increased, leading to better detection performance. This trend was verified in [12]. This leads to better image quality as well as a lower injected dose. Thus, a primary conclusion that can be drawn is that the better the time resolution of the coincidence spectrometer, the better is the gain and spatial resolution.

We determined that f values for a heavy body (i.e., heavy patient), as shown in figure 12 and (2), are always higher than those of the gains of an average body and brain. This means that the constructed TOF–PET system has an advantage for heavy patients as it has a better timing resolution because of faster scintillators and PMTs.

It was found that f values for heavy bodies, average bodies and brains were highest at 6 cm because the best time resolution was obtained at this distance (figure 13). In addition, this shows that the position of the stop detector has the best detection efficiency. Thus, the distance between the stop detector and radio pharmaceutics position should be an optimal value to achieve the best detection performance and better image quality, as the optimal patient position for the use of radio pharmaceutics, especially in planning tests with the body or organ phantoms, was extremely effective.

6. Conclusion

In our previous studies, in which TOF–PET measurements were conducted [21,22], we used different types of PMTs (Burle Model 8575) and scintillation crystals (BC412, BC418) to obtain the best time resolution values for the coincidence spectrometers we examined. In these studies, the PMTs used to be slow even though the crystals exhibited short decay times. Therefore, the time resolution results obtained in this study were better than those of the previous studies. For this reason, we have chosen new generation PMTs applicable to PET systems [31]. Moreover, selected scintillation crystals had shorter decay times in this study compared to previous studies [21,22]. When these results are considered together, enhancing the time resolution of the coincidence spectrometer is clearly necessary to increase the image quality. Therefore, to achieve the best image quality in a TOF–PET system, faster scintillation crystals and PMTs used together with optimal patient positions are highly recommended. In addition, these parameters help to reduce the injected dosages for patients and detect small lesions.

Acknowledgement

This work was supported by the Scientific and Technological Research Council of Turkey (TUBITAK) under Project No. 116F324.

References

[1] M N Wernick and J N Aarsvold, *Emission tomography: The fundamentals of PET and SPECT* (Elsevier Academic Press, USA, 2004)
[2] International Atomic Energy Agency, *Quality assurance for PET and PET/CT systems* (IAEA Human Health Series No. 1, Vienna, 2009)
[3] M M Khalil, *Basic sciences of nuclear medicine* (Springer-Verlag, Germany, 2011)
[4] R A Powsner, M R Palmer and E R Powsner, *Essentials of nuclear medicine, physics and instrumentation* (John Wiley & Sons, USA, 2013)
[5] Hamamatsu Photonics Photomultiplier Tubes for PET, http://www.hamamatsu.com/eu/en/product/application/1501/3503/3001/index.html#pmt_1_en=0
[6] M Moszynski and B Bengtson, *Nucl. Instrum. Methods* **158**, 1 (1979)
[7] W S Choong, *Phys. Med. Biol.* **54**, 6495 (2009)

[8] J S Karp, S Surti, M E Daube-Witherspoon and G Muehllehner, *J. Nucl. Med.* **49**, 462 (2008)
[9] W W Moses, *IEEE Trans. Nucl. Sci.* **50**, 1325 (2003)
[10] W W Moses, *Nucl. Instrum. Methods A* **580**, 919 (2007)
[11] M Conti, B Bendriem, M Casey, M Chen, F Kehren, C Michel and V Panin, *Phys. Med. Biol.* **50**, 4507 (2005)
[12] M Conti, *Phys. Med.* **25**, 1 (2009)
[13] M E Casey, http://scipp.ucsc.edu/~hartmut/UFSD/Simens_ultraHD-PET_White_Paper.pdf
[14] S Vandenberghe, E Mikhaylova, E D'Hoe, P Mollet and J S Karp, *EJNMMI Phys.* **3**, 1 (2016)
[15] J T Bushberg, J A Seibert, E M Leidholdt and J M Boone, *The essential physics of medical imaging* (William-Wilkins, USA, 2001)
[16] J J P De Lima, *Nuclear medicine physics* (Taylor & Francis, USA, 2011)
[17] T Budinger, *J. Nucl. Med.* **24**, 73 (1983)
[18] F Collamati, *An intraoperative beta-probe for cancer surgery*, Ph.D. thesis (Sapienza University, 2016)
[19] A Ferrari, P R Sala, A Fasso and J Ranft, *Fluka: A multi-particle transport code*, CERN INFN/T_05/11: SLAC-R-773, 2005
[20] G Battistoni, F Cerutti, A Fasso, A Ferrari, S Muraro, J Ranft, S Roesler and P R Sala, *AIP Conf. Proc.* **896**, 31 (2007)
[21] E E Ermis, C Celiktas and E Pilicer, *Radiat. Meas.* **62**, 52 (2014)
[22] E E Ermis, C Celiktas and E Pilicer, *Rev. Sci. Instrum.* **87**, 053504 (2016)
[23] M E Phelps, *PET physics, instrumentation, and scanners* (Springer, USA, 2006)
[24] Saint-Gobain Scintillators, *Organic scintillation materials and assemblies*, https://www.crystals.saint-gobain.com/sites/imdf.crystals.com/files/documents/sgc-organics-plastic-scintillators.pdf
[25] S N Ahmed, *Physics and engineering of radiation detection* (Elsevier, Netherlands, 2015)
[26] R W Leo, *Techniques for nuclear and particle physics experiments* (Springer-Verlag, Germany, 1987)
[27] N Tsoulfanidis, *Measurements and detection radiation* (Taylor & Francis, USA, 1995)
[28] G F Knoll, *Radiation detection and measurement* (John Wiley & Sons. Inc, New York, 2000)
[29] Hamamatsu Photonics KK, *Photomultiplier tubes basics and applications*, https://www.hamamatsu.com/eu/en/product/type/R1828-01/index.html
[30] Ortec Model VT120, *Fast timing preamplifier operating and service manual*, https://www.ortec-online.com/-/media/ametekortec/brochures/vt120.pdf
[31] M O Bedwell and T J Paulus, *IEEE Trans. Nucl. Sci.* **23**, 234 (1976)
[32] M Conti, *Eur. J. Nucl. Med. Mol. Imaging* **38**, 1147 (2011)
[33] J Torres, R Garcia, A Aguilar, J Soret, J Martos, A J Gonzalez, F Sanchez, J M Benlloch and M J Rodriguez, *Implementation of TOF-PET systems on advanced reconfigurable logic devices* (Intech, Croatia, 2013)